

ORIGINAL RESEARCH

Open Access



# Effect of MnO<sub>2</sub>-biochar composites on promoting humification during chicken manure composting

Haishi Qi<sup>2</sup>, Wenfang Gao<sup>1</sup>, Lina Xie<sup>1</sup>, Guogang Zhang<sup>1</sup>, Caihong Song<sup>3</sup>, Zimin Wei<sup>1\*</sup>, Ning Hu<sup>4</sup> and Tong Li<sup>2</sup>

## Abstract

The present study aimed to accelerate the humification and to investigate how MnO<sub>2</sub> modification of biochar (MBC) drives the humus formation during composting with chicken manure. In this study, compared with the control group (CK), the addition of MBC caused an increase in the concentration of both humus and humic acid (HA), with a respective enhancement of 29.1% and 37.2%. In addition, MBC also improved the stability of compost products. Hetero two-dimensional correlation spectra further exhibited that the MBC could alter the formation mechanism of humus fractions during composting. Random forest analysis showed that *Microbacterium*, *Bacteroides*, *Kroppenstedtia*, *Gracilibacillus*, and *Lentibacillus* were significantly related to humus formation ( $P < 0.05$ ). MBC enhanced the absolute abundance of these five genera during composting. The structural equation model further confirmed that these five genera could be indirectly involved in humus formation, through the production of aromatic compounds via secondary metabolism. Additionally, these five genera could directly transform organic components into macromolecular humus structures. Therefore, the increase in these five genera might be a direct response to the acceleration of the humification during MBC composting. These findings demonstrate the potential value of MBC in harmless disposal of hazardous biowastes through composting.

## Highlights

- MnO<sub>2</sub> modification of biochar changed the formation mechanism of humus fractions.
- Key genera involved in humus formation were identified.
- Among of MnO<sub>2</sub> modification of biochar, key genera and humus formation were revealed.

**Keywords** Composting, MnO<sub>2</sub>-biochar, Humus, Key microbes

Handling editor: Lukáš Trkal

\*Correspondence:

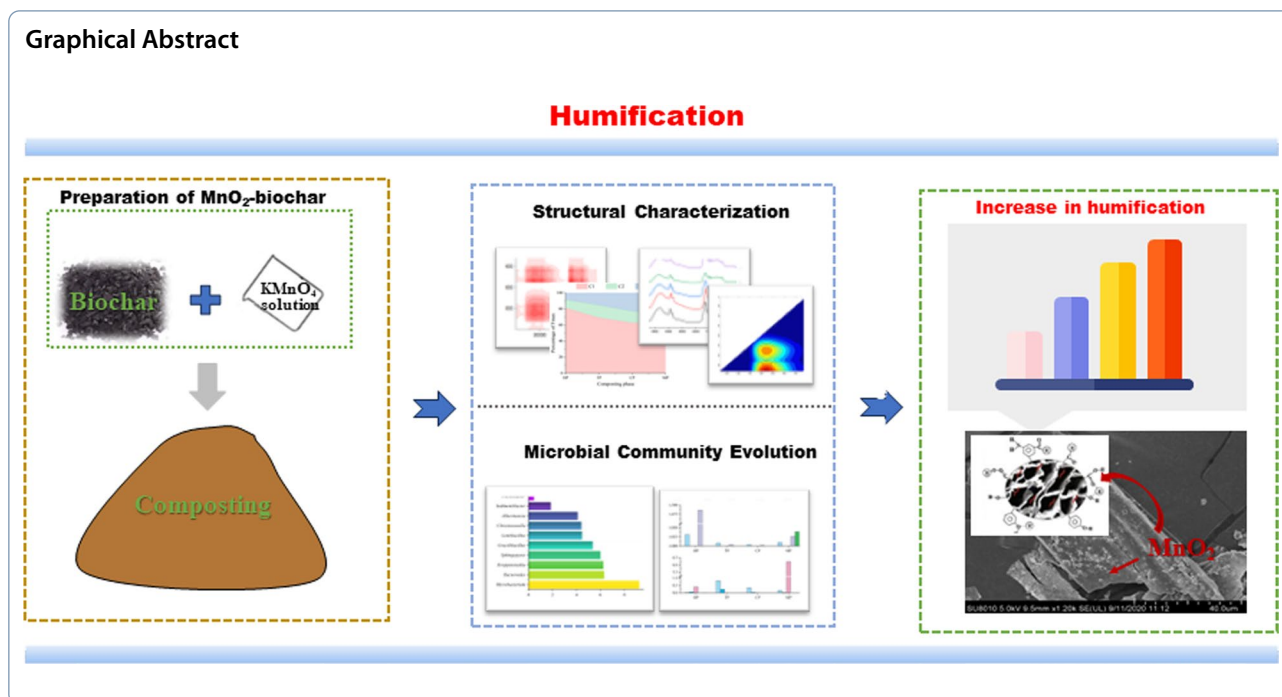
Zimin Wei

zmwei@tjnu.edu.cn

Full list of author information is available at the end of the article



© The Author(s) 2024. **Open Access** This article is licensed under a Creative Commons Attribution 4.0 International License, which permits use, sharing, adaptation, distribution and reproduction in any medium or format, as long as you give appropriate credit to the original author(s) and the source, provide a link to the Creative Commons licence, and indicate if changes were made. The images or other third party material in this article are included in the article's Creative Commons licence, unless indicated otherwise in a credit line to the material. If material is not included in the article's Creative Commons licence and your intended use is not permitted by statutory regulation or exceeds the permitted use, you will need to obtain permission directly from the copyright holder. To view a copy of this licence, visit <http://creativecommons.org/licenses/by/4.0/>.



## 1 Introduction

Chicken manure, a typical agricultural biowaste, is produced in large quantities every year, causing a series of environmental problems, such as pathogen transmission and antibiotics enrichment (He et al. 2022). To address this issue, composting has been proved an effective approach, because it reuses resources while disposing the biowaste in a safe way (Ji et al. 2023; Wu et al. 2021). In the process, organic matter is converted into stable compost products rich in humus, which are good soil amendments and organic fertilizers (Sun et al. 2023; Zhang et al. 2022a). Compost product with high levels of humus has numerous positive benefits in the treatment of hazardous biowaste, particularly complex organic pollutants (Song et al. 2022; Yuan et al. 2018). Therefore, humus content and aromatization degree are key indicators to determine the environmental effect of compost products. In traditional composting, the formation of humus is limited, because part of organic matter is mineralized (for example, turned into  $CO_2$  or  $CH_4$ ) through the metabolic activity of microbes (Chen et al. 2020). For this reason, an efficient approach is needed to promote humus formation during composting, which can be beneficial for resource utilization of agricultural biowastes.

Various research has been conducted to reduce carbon losses and promote humification (including quantity and quality) in composting (Pan et al. 2009; Xiong et al. 2023; Zhang et al. 2023). Among them, biochar has garnered significant attention for its positive impact as a compost

amendment (Lyu et al. 2020; Zhang et al. 2022b). Biochar can improve composting through enhancing microbial activity, moisture retention, and nutrient availability (Oldfield et al. 2018). Additionally, biochar can provide a physical substrate for microbial colonization (Zhao et al. 2022b). Most importantly, the collaborative utilization of biochar and compost products are more effective in improving soil fertility and promoting carbon sequestration through their unique physical and chemical properties (Awasthi et al. 2017; Wang et al. 2017). However, biochar produced through conventional high-temperature pyrolysis techniques exhibits a diminished specific surface area, restricted pore structure, and a reduced variety of surface functional groups, consequently resulting in inferior functional properties (Rajapaksha et al. 2016). Consequently, in order to address the constraints of pristine biochar, various studies have been conducted to enhance its functional characteristics through modification.

The primary techniques utilized to modify biochar include physical modification, chemical modification, and impregnation with metal oxides (Liang et al. 2017b; Liu et al. 2020b). Physical modification involves altering the structure of biochar through mechanical or thermal treatments (El-Naggar et al. 2022). These treatments can improve the porosity, surface area, and water-holding capacity of biochar, making it more effective for specific applications (El-Naggar et al. 2022). Chemical methods mean adding chemicals to biochar, such as acids, bases,

or salts, to alter its chemical properties. For instance, nitrogen-rich compounds like urea or ammonium sulfate can raise the biochar's ability to retain nutrients and elevate soil fertility (Kasera et al. 2021). However, both physical and chemical modifications have limitations, including reduced effectiveness, heavy pollution, or high cost (Liu et al. 2020a). Over the years, researches have focused on impregnating biochar with metal oxides to improve its properties, such as MgO, Fe<sub>2</sub>O<sub>3</sub>, AlOOH, MnO<sub>x</sub>, and so on (Liang et al. 2015; Shaheen et al. 2022; Zhang et al. 2012). It has many merits. Firstly, metal oxide nanoparticles can improve the physicochemical properties of biochar (Shaheen et al. 2022). Additionally, metal oxide modification imparts catalytic properties to biochar, enabling it to facilitate chemical reactions (Shaheen et al. 2022). As catalysts, metal oxides facilitate the conversion of certain compounds or the breakdown of complex molecules (Hardie et al. 2009). MnO<sub>x</sub> is one such strong catalyst, particularly in promoting humification in composting (Qi et al. 2021). Accordingly, MnO<sub>x</sub>-modified biochar (MBC) may have great potential in optimizing composting substrates and promoting humification. However, this potential remains unexplored.

Therefore, this paper explores the effect of MBC on humification process in the composting. Here, (1) the effects of MBC on the formation of humus fractions were assessed; (2) the mechanism of humus formation was revealed; (3) the potential mechanism of MBC in promoting humus formation in composting was explored.

## 2 Materials and methods

### 2.1 Preparation of functional materials

Biochar was obtained through the following steps: the corn straw was pyrolyzed in a high temperature atmosphere furnace in an oxygen-free atmosphere at a heating rate of 5 °C min<sup>-1</sup> and held at 200 °C for 2 h. MnO<sub>2</sub> (pure 85%) was purchased from the Xilong Chemical Company, Guangdong, China. The MnO<sub>2</sub>-biochar composite (MBC) was prepared using Liang et al.'s (2017a, b) method, with modifications. Initially, biochar (90 g) and KMnO<sub>4</sub> (3.16 g) were combined in 900 mL ultrapure-water at 25 °C. The resulting mixture was then subjected to ultrasonic oscillation for a duration of 0.5 h. Subsequently, a solution of Mn (II) acetate tetrahydrate with a concentration of 0.3 M in 100 mL was added drop by drop while stirring the mixture, resulting in the formation of MnO<sub>2</sub> (dark brown) within the mixed solution. Following this, the mixtures were heated to a temperature of 80 °C and held for a duration of 30 min, allowing for the formation of the MBC suspension prior to filtration. Eventually, MBC was washed multiple times with ultrapure-water and subsequently dried at a temperature of 80 °C.

Additionally, the morphology of the MBC was characterized through scanning electron microscopy. The results showed that MnO<sub>2</sub> has successfully adhered to the biochar (Additional file 1: Fig. S1).

### 2.2 Composting trials

Chicken manure (CME) and corn straw (CSW) were selected as the composting materials and were obtained from a local farm in Harbin, China. CSW (1–2 cm) was used as a compost conditioner. The basic information of CME and CSW is shown in Additional file 1: Table S1. The mass ratio of CME to CSW in the mixture was 2:1 (dry weight) in order to attain the C/N ratio (about 25~30:1) for the composting. Composting trials were conducted for a duration of 45 days, utilizing lab-scale reactors with a working volume of 12.5 L. These reactors were equipped with a temperature control system (Additional file 1: Fig. S2), the specifics of which are outlined in Zhao et al.'s (2016) study. Five treatments were designed, namely 5% biochar (B), 0.05% MnO<sub>2</sub> (M), the mixture of 5% biochar and 0.05% MnO<sub>2</sub> (M+B), and 0.05% MnO<sub>2</sub>-5% biochar composites (MBC) were added based on the dry weight of raw materials as per requirement for each treatment, which were composts without additives were designed as control groups (CK). There were three replicates per treatment. The initial moisture level and aeration of each treatment were held at approximately 60% and 0.5 L (kg DM min)<sup>-1</sup>. Compost products were taken on Day 0, 3, 10, 18, 25, 35, and 45 to analyze the physicochemical properties. According to the change of temperature, samples on days 3, 10, 18, and 35 were chosen as the samples of the heating phase (HP), thermophilic phase (TP), cooling phase (CP), and maturity phase (MP), respectively, which were applied to microbial succession analysis.

### 2.3 Humification

Organic matter (OM) was measured by determining the dry weight loss after ignition at 550 °C in a muffle furnace for 5.5 h. The calculation formula is as follows:

$$\text{OM content(\%)} = \frac{X_0 - X_1}{X_0}$$

(X<sub>0</sub> = sample contents before burning; X<sub>1</sub> = sample contents after burning).

Humus was extracted and measured using methods described previously (Qi et al. 2021). Briefly, shaking with a 200 mL 0.1 M solution (NaOH + Na<sub>4</sub>P<sub>2</sub>O<sub>7</sub>) at 150 rpm min<sup>-1</sup> for a duration of 24 h. The solid-liquid mixture was separated by 20-min centrifugation at 12,000 rpm. The liquid was filtered through a 0.45-μm Millipore filter. Subsequently, the liquid's pH was manipulated to 1 by employing 6 M HCl, following which the solution

was placed at 4 °C for a duration of 12 h to induce humic acid (HA) precipitation. The supernatant was separated by another 20-min centrifugation at 12,000 rpm, yielding flavic acid (FA). Purification of FA was conducted utilizing Amberlite XAD-8 resin. Finally, SHIMADZU TOC-Vcph analyzer was utilized to determine the carbon content of both HA and FA.

#### 2.4 Spectroanalysis

All HA samples (carbon concentration) were manipulated to 10 mg L<sup>-1</sup> using ultrapure water. The fluorescence spectra of all HA samples were acquired utilizing a Hitachi F-7000 spectrophotometer from Japan. Emission (Em) and excitation (Ex) wavelengths (220–600 nm) were recorded in 5 nm intervals. The scan speed was set at 2400 nm min<sup>-1</sup>. To mitigate the contribution of Rayleigh and Raman scattering, the fluorophore of samples was adjusted by subtracting the fluorophore of Milli-Q water. Moreover, the fluorescence intensities of all samples were characterized using maximum fluorescence intensity (*F<sub>max</sub>*).

One milligram of powdered HA sample was analyzed by flourier transform infrared (FTIR). The FTIR spectra were collected in the ranges of 4000–400 cm<sup>-1</sup> with Tensor II spectrometer (Bruker Co., Germany). The resolution of spectrometer was 0.9 cm<sup>-1</sup>, and signal to noise ratio was > 50. Additionally, all FTIR spectra were smoothed, and baseline-corrected.

#### 2.5 Microbiological analyses

Fresh compost samples collected at days 3, 10, 18, and 35 were used to extract DNA with a Fast Soil DNA Kit (Omega Biotek, Inc.). Primers 341F and 806R were utilized to amplify the V3-V4 regions of the 16S rRNA gene as described previously (Chen et al. 2022). Sequencing was analyzed using the platform of Illumina HiSeq. Raw sequence data underwent filtering to obtain “Clean Data” using QIIME 1.9.1. Subsequently, the filtered sequences were assigned into operational taxonomic units (OTUs) at a 97% sequence identity with the assistance of the UPARSE 7.0.1. Additionally, the absolute abundance of key microbes was provided from the platform of Illumina HiSeq. Briefly, the absolute abundance in high-throughput sequencing is typically calculated by aligning the sequencing reads of each sequence to the corresponding gene or sequence in a reference genome, and then calculating the abundance based on the alignment results.

#### 2.6 Statistical analysis

MATLAB 2013a DOM Fluor toolbox was employed for conducting parallel factor analysis (PARAFAC), as previously described by He et al. (2013). Two-dimensional correlation spectra (2DCOS) and hetero-2DCOS analyses

were performed using 2D Shige software (He et al. 2013). To identify the change of the bacterial community structure, non-metric multidimensional scaling (NMDS) was performed using Canoco (Version 5.0). Random Forest models were graphically visualized using R 4.0.2. Lastly, a structural equation model (SEM) was implemented with AMOS 23.0 to assess the causality among the bacterial community, physicochemical properties, and humus components.

### 3 Results and discussion

#### 3.1 Variations in humification parameters

The quality of compost products can be effectively assessed through the quantification of OM, humus, HA, and FA alterations (Fig. 1). The content of OM decreased in the whole composting (Fig. 1a), probably because OM could be degraded into CO<sub>2</sub> or transformed into humus by microbial metabolic activity (Zhao et al. 2017). On the 45th day, OM content decreased by 21.0%, 24.2%, 25.0%, 27.0%, and 19.0% at CK, B, M, M+B, and MBC, respectively (Fig. 1a). This result suggested that there was no significant difference between MBC treatment and the CK ( $P > 0.05$ ). Humus concentration decreased slightly in the first 25 days (Fig. 1b), which was caused by the fact that the labile substances of humus were used by microorganisms to support their metabolic activity in the first 25 days. During the maturity phase, humus concentration exhibited an increase in all treatments due to the continuous transformation of OM (Fig. 1b). On the 45th day, the humus concentrations of CK, B, M, M+B, and MBC were 55.4 mg g<sup>-1</sup>, 50.2 mg g<sup>-1</sup>, 67.1 mg g<sup>-1</sup>, 41.3 mg g<sup>-1</sup>, and 71.5 mg g<sup>-1</sup>, respectively (Fig. 1b). Humus content of M and MBC increased by 21.1% and 29.1%, respectively. Meanwhile, the HA content of M and MBC was higher 11.1% and 37.2% than that in the CK (Fig. 1c), and the degradation of FA slowed down in M and MBC treatments (Fig. 1d). Therefore, in this study, the addition of MnO<sub>2</sub> and MnO<sub>2</sub>-biochar composites could promote humification during composting, while the biochar and the mixtures of biochar and MnO<sub>2</sub> accelerated organic component mineralization. Studies have shown that biochar could promote microbial growth and therefore promote organic component degradation (Zhao et al. 2022a). MnO<sub>2</sub> could promote the humus formation from simple compounds by stimulating chemical reactions (Hardie et al. 2009). Interestingly, the concentration of humus was found to be the lowest in the M+B group (Fig. 1b). The MnO<sub>2</sub> can form complexes or stable Mn-O-R (R: functional groups) with the anions or functional groups derived from biochar, thereby limiting their functionality (Liang et al. 2017b). Research has shown that MBC has a rough surface, larger surface area and pore volume compared to biochar, and exhibits better catalytic

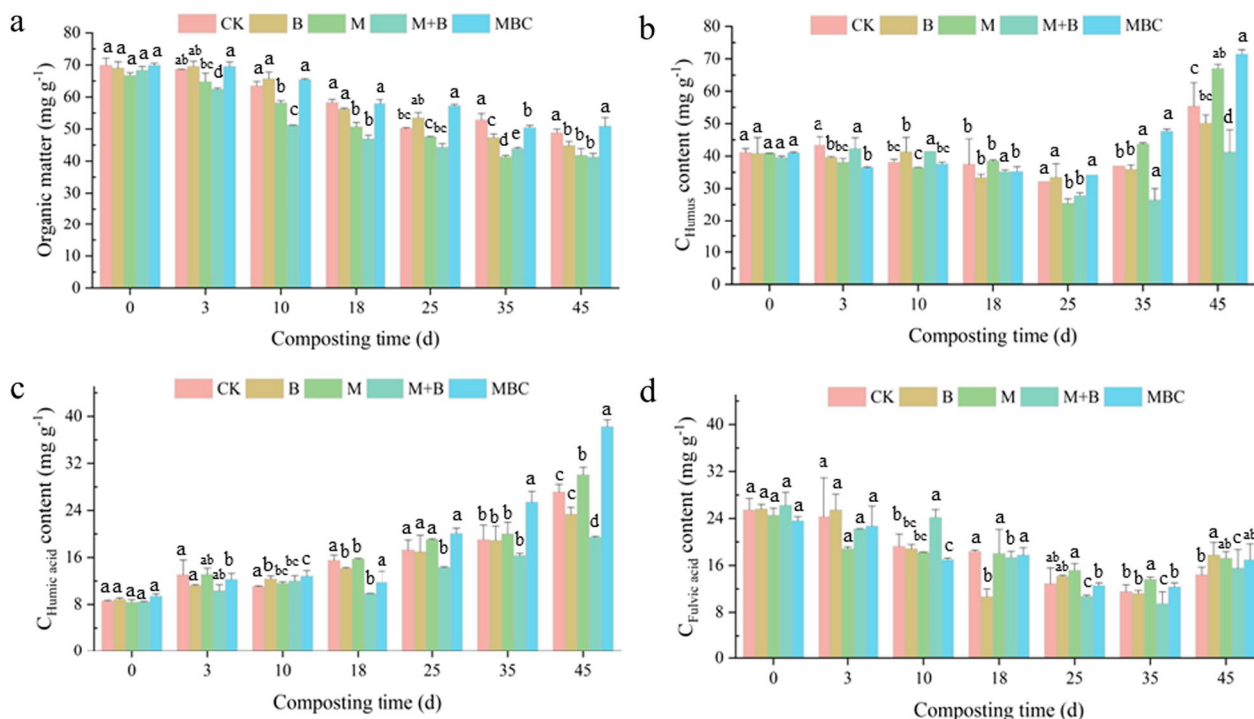


**Fig. 1** Changes in humification index during composting. **a–d** correspond to the organic matter (OM), humus, humic acid (HA), and fulvic acid (FA), respectively. The results are the mean of three replicates, and the error bars indicate standard deviation. Different letters indicate significant differences among treatments using Tukey’s HSD test at  $P < 0.05$

performance than MnO<sub>2</sub> (Liang et al. 2017b; Shaheen et al. 2022). Therefore, MnO<sub>2</sub>-biochar composites could effectively promote the humification of compost products. This section investigates the impact of MBC on the quantity of humus, followed by an analysis of structural evolution.

### 3.2 Analysis of the fluorescent component in HA

The structural characteristics of HA can directly reflect the evolution of humus structure in composting. Using PARAFAC modeling, the fluorescence spectra of HA were segregated into three distinct components (Fig. 2). The peak position of component 1 (C1) from all treatments was at 220 (280) nm/330 nm. The position of C1 in HA resembled that of tryptophan-like substances, which have been previously identified as protein-like components (He et al. 2014). The peak position of component 2 (C2) from CK was at 260 nm/410 nm, whereas the peak of C2 originating from the B, M, M+B, and MBC groups exhibited a red-shift (shift towards longer wavelengths) and occurred at 260 nm/445 nm. This study attributed C2 to humic-like substances generated from organic matter because of microbial activities during composting (He et al. 2014). The peak position of component 3 (C3) from CK was at 250 nm/510 nm, but that of C3 from B, M+B, and MBC groups red-shifted to 260 nm/530 nm.

This component in this study should be mainly attributed to terrestrial humic-like peaks (He et al. 2014). Molecular weight and humification degree of these components were found to have a positive relationship with the peak wavelength of the fluorescence results (He et al. 2013). According to the wavelength of the peak position of fluorescence components, the humification degree of the HA components decreased in the order: C3 > C2 > C1.

The variation in *F<sub>max</sub>* of HA during composting is depicted in Additional file 1: Fig. S3. The *F<sub>max</sub>* of C1 exhibited a significantly higher value compared with that of C2 and C3 in the CK group (Additional file 1: Fig. S2a) ( $P < 0.05$ ), suggesting that HA structure of CK had a low humification degree and was easy to be utilized by microorganisms during composting. However, the *F<sub>max</sub>* of C2 and C3 was higher than that of C1 for the B (56.1%), M (73.7%), M+B (56.2%), and MBC (85.5%) groups (Additional file 1: Fig. S2b–e). These results demonstrated that these function materials could increase the humification degree of HA during composting, with the MBC treatment exhibiting the most favorable performance in this study. Therefore, MnO<sub>2</sub>-biochar composites showed best performance in improving the quality and quantity of humus fractions during composting. In addition to the core aromatic carbon skeleton, HA exhibits a rich variety of functional groups on its

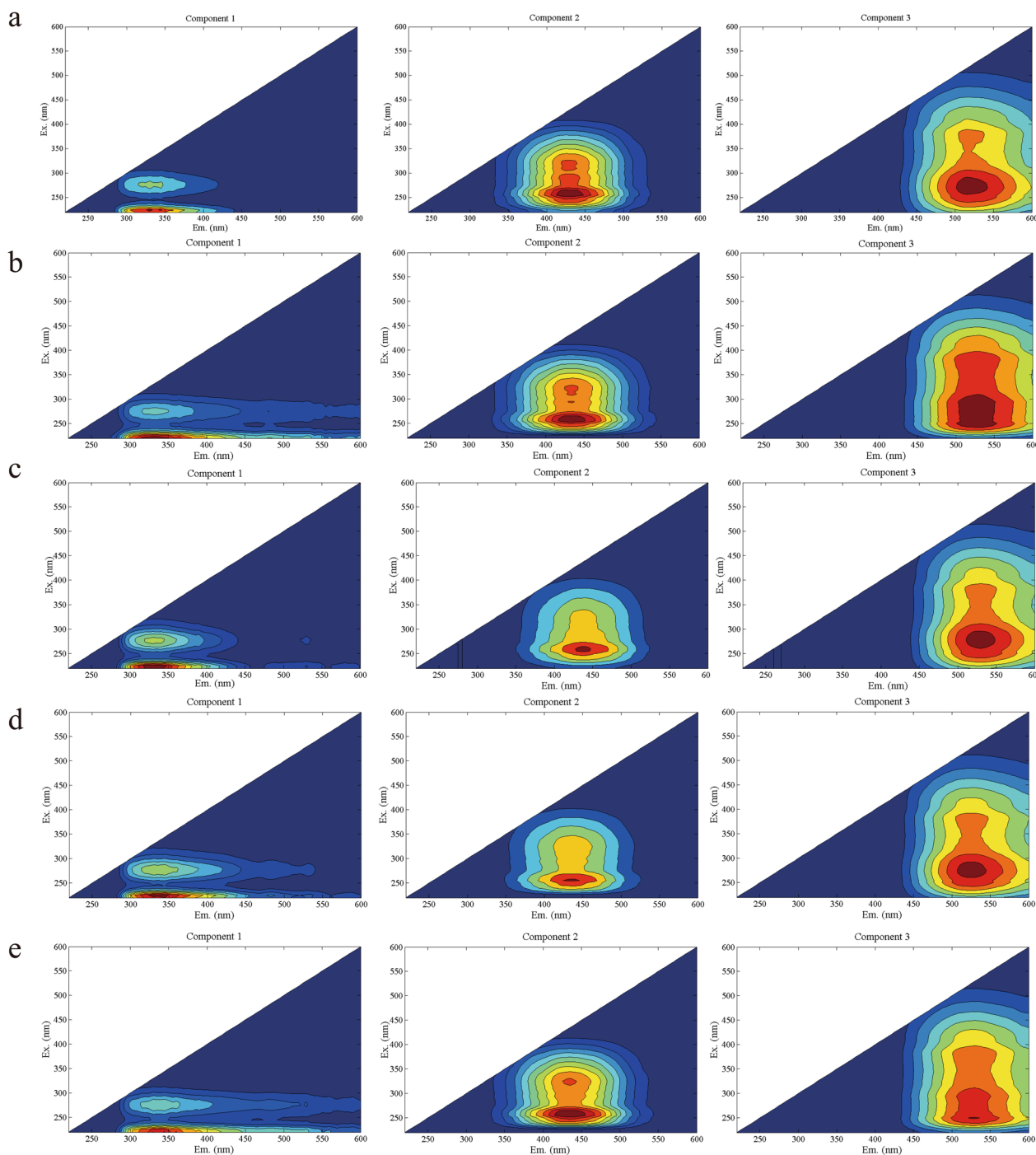


**Fig. 2** During the composting, the PARAFAC model identified fluorescent components of HA. **a–e** correspond to the CK, B, M, M+B, and MBC groups, respectively

surface structure. Therefore, FTIR spectroscopy is further employed to determine the functional group composition and evolution of HA.

### 3.3 Effect of MnO<sub>2</sub>-biochar composites on the infrared functional group of HA

#### 3.3.1 Evolution of infrared functional groups

FTIR spectroscopy is employed as a valuable tool for examining the variation in functional groups throughout

the composting process. The FTIR spectroscopy analysis revealed that the CK and MBC groups exhibited similar absorbance peaks (Additional file 1: Fig. S4). The stretching vibration of OH groups in carboxylic acids, phenols, or alcohols could be attributed to a band observed at  $3280\text{ cm}^{-1}$  (Zhang et al. 2021). Two minor bands observed at  $2950\text{ cm}^{-1}$  and  $2846\text{ cm}^{-1}$  were commonly associated with the stretching vibrations of C-H bonds in aliphatic compounds (Gao et al. 2019), and the intensities of them declined by Day 45. This could be attributed to the microbial-mediated degradation of aliphatic compounds during composting. The absorption bands at  $1650\text{ cm}^{-1}$  were commonly associated with C=O stretching of quinone (Yang et al. 2019), and the peak intensity of MBC was observed to be higher than that of CK on Day 45. A weak absorption band at  $1540\text{ cm}^{-1}$  was related to the presence of amide II bonds in proteins (Zhang et al. 2021). A band centered at  $1420\text{ cm}^{-1}$  was commonly associated with the C-H deformation of lignin and hemicellulose (Gao et al. 2019). A band centered at  $1250\text{ cm}^{-1}$  could be assigned to phenols, aldehydes and aromatic ethers (Zhang et al. 2021); A band centered

at  $1080\text{ cm}^{-1}$  was related to the stretching vibration of C-O bonds in carbohydrates or polysaccharide-like substances. (Gao et al. 2019). These results showed that HA was rich in protein, polysaccharide, aliphatic and lignin compounds, which was consistent with previous studies (Gao et al. 2019). Additionally, the  $\text{MnO}_2$ -biochar composites improved the formation of aromatic carbon skeleton during composting.

### 3.3.2 Conversion order of HA functional group

The complex structure of HA limits the ability of FTIR spectra to provide comprehensive insights into the evolution of it. Therefore, 2DCOS was employed to further reveal the conversion information of HA functional group over composting time (Fig. 3). In the synchronous maps, two auto-peaks ( $1650\text{ cm}^{-1}$  and  $3280\text{ cm}^{-1}$ ) were found in the CK groups, and four auto-peaks ( $3280\text{ cm}^{-1}$ ,  $2846\text{ cm}^{-1}$ ,  $1650\text{ cm}^{-1}$ , and  $1250\text{ cm}^{-1}$ ) were observed in the MBC groups. Additionally, all cross-peaks in the synchronous maps of CK and MBC groups were positive, suggesting that the changes of functional groups were in the same direction. The asynchronous maps of CK and

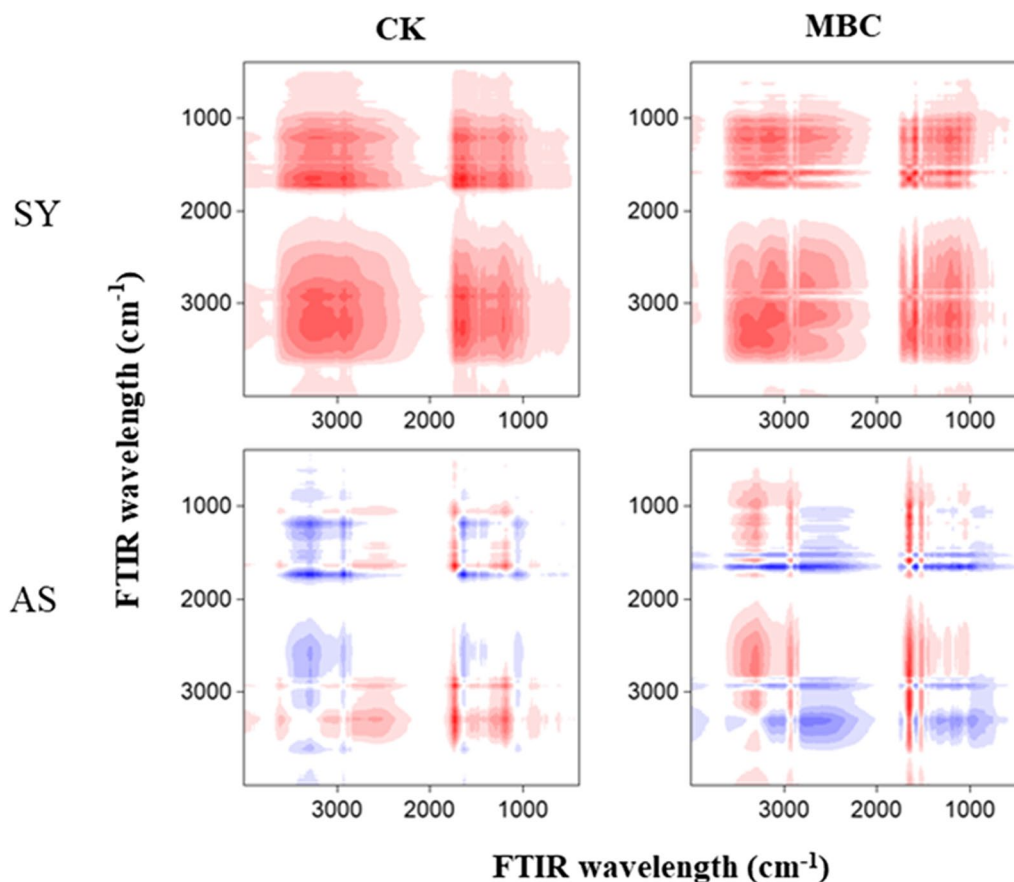


**Fig. 3** Synchronous maps were generated by conducting 2D hetero-spectral correlation analysis of the FTIR and EEM spectra of HA. In the visualization, red and blue indicate positive and negative correlations, respectively, with a more intense color reflecting a stronger correlation

MBC showed significant differences. In the asynchronous maps of CK groups, 4 positive cross-peaks were found at (1080, 1250–3280), (1250, 1650), (1420, 1650), and (1540, 1650), and 5 negative cross-peaks were detected at (1250, 1420–3280), (1420, 2846–3280), (1540, 2846–3280), (1650, 2846–3280), and (2846, 3280). According to Noda's rule, the change of HA functional groups in CK followed the sequence:  $1080\text{ cm}^{-1} > 3280\text{ cm}^{-1} > 2846\text{ cm}^{-1} > 1540\text{ cm}^{-1} > 1420\text{ cm}^{-1} > 1250\text{ cm}^{-1} > 1650\text{ cm}^{-1}$ , corresponding to C–O stretching of polysaccharose-like substances > phenolic OH > aliphatic C–H bands > amide II bonds in proteins > C–H deformation of lignin and hemicellulose > aromatic ethers > C=O stretching of quinone. These results showed that during CK composting, polysaccharides might bind to phenolic compounds through aldehyde groups, low molecular proteins might bind to carbon skeleton by amido linkage, low molecular carbohydrates and aliphatic compounds might combine with carbon skeleton through ether bands, and eventually, many such units are polymerized into HA macromolecular structures.

In the asynchronous maps of MBC groups, 8 positive cross-peaks were found at (1080, 1250–3280), (1250, 1540), (1250, 1650), (1250, 1420), (1250, 3280), (1420, 1540), (1420, 1650), (1540, 1650), and 7 negative cross-peaks were detected at (1250, 1420), (1420, 2846), (1420, 3280), (1540, 2846), (1650, 2846), (1650, 3280), and (2846, 3280). Therefore, the change of HA functional groups in MBC followed the order:  $1080\text{ cm}^{-1} > 3280\text{ cm}^{-1} > 2846\text{ cm}^{-1} > 1250\text{ cm}^{-1} > 1420\text{ cm}^{-1} > 1540\text{ cm}^{-1} > 1650\text{ cm}^{-1}$ , corresponding to C–O stretching of polysaccharose-like substances > phenolic OH > aliphatic C–H bands > aromatic ethers > C–H deformation of lignin and hemicellulose > amide II bonds in proteins > C=O stretching of quinone. These results indicated that C=O stretching of quinone appeared after amide II bonds in proteins during MBC composting, suggesting that quinone and proteins might be condensed into HA through the Maillard reaction. Therefore, the addition of MnO<sub>2</sub>-biochar composites did not change the structural composition of HA but its formation mechanism. Additionally, considering the HA content increased, the binding mode of functional groups in MBC might be more effective.

### 3.4 Dynamics of bacterial community during composting

The relative abundances of bacterial communities (phylum level) during composting are displayed in Fig. 4a. Before the mature phases of composting, *Firmicutes* (relative percentage around 90.0%) was dominant phylum in CK and MBC treatments. Its dominance might be because *Firmicutes* was able to tolerate high temperatures and harsh conditions in composting (Zhang et al. 2021). In the mature phases of composting, however, the relative

percentage of *Firmicutes* decreased to 17.8% and 49.2%, and the relative percentage of *Proteobacteria* increased to 63.2% and 24.1% in CK and MBC treatments, respectively. Researchers have proved that *Proteobacteria* was an important driver of low-molecule nutrients degradation in composting (Awasthi et al. 2017). Therefore, the MnO<sub>2</sub>-biochar composites addition increased the relative percentage of *Firmicutes* and decreased the relative percentage of *Proteobacteria* in the mature phases of composting (Fig. 4a). These results demonstrated that the MnO<sub>2</sub>-biochar composites might contribute to the low-molecule organic matter sequestration during composting. Random forest model was employed to predict the key bacterial community involved in humus formation at genus level (Fig. 4b). The result showed that only 5 genera, *Microbacterium*, *Bacteroides*, *Kroppenstedtia*, *Gracilibacillus*, and *Lentibacillus*, were significantly related to humus formation during composting ( $P < 0.05$ ). They were called key genera in this study. The MnO<sub>2</sub>-biochar composites addition enhanced the absolute abundance of key genera in maturity period of compost (Fig. 4c), which might be one main biological reason for the humus content increase in MBC treatments. Furthermore, the addition of MnO<sub>2</sub>-biochar composites resulted in a reduced dissimilarity in the distance matrices of bacterial community structure between different periods, in comparison with the CK (Fig. 4d). Closer distance matrices suggested similarity in the function of bacterial community in MBC treatments. In short, the introduction of MnO<sub>2</sub>-biochar composites disrupted the equilibrium of the native bacterial community, leading to a notable alteration in both richness and structure.

### 3.5 The possible mechanism of humus formation

The SEM was further applied to investigate the possible mechanism of humus formation in this study (Fig. 5). Key bacteria were found positively related to functional groups of aromatic compounds and humus formation in composting, suggesting that they might be produced through the bacteria's secondary metabolites. Aromatic compounds were significantly correlated with fluorescent components formation, probably because the aromatic compounds could be condensed into a stable humus structure. Additionally, both were positively related to humus formation during composting. This further confirmed that aromatic compounds were the carbon skeleton of humus (Lodygin et al. 2014). Another point is that  $\beta$  diversity were found negatively related to functional groups of aromatic compounds formation during composting. This might be because rich  $\beta$  diversity was not conducive to the preservation of organic components (Liang et al. 2017a). Accordingly, key microbes might mediate the formation of humus in two ways: one was



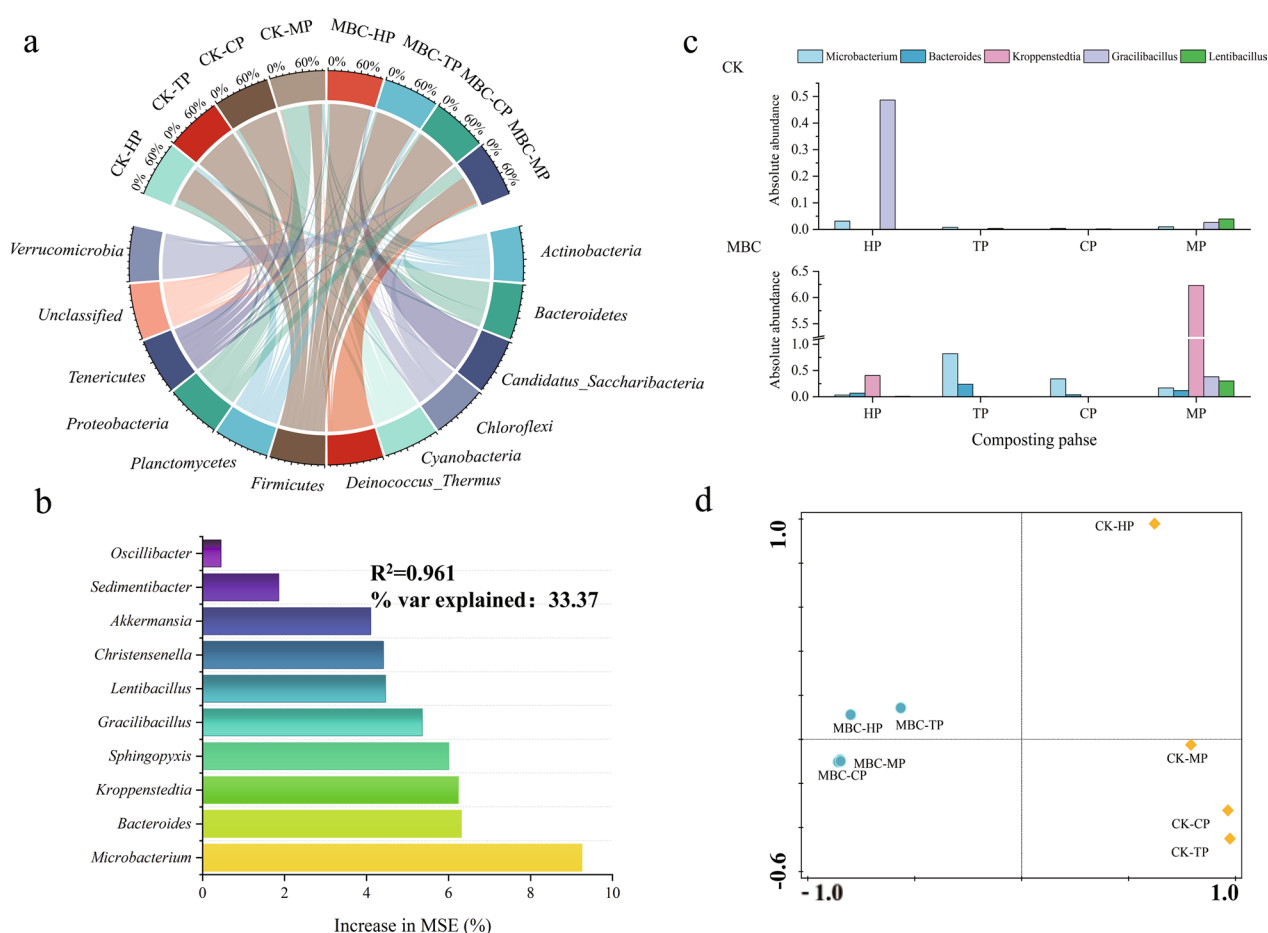


**Fig. 4** Changes in the bacterial community during composting. **a** depicts the distribution of phyla, while **b** shows the key genus predicted by random forest. Additionally, **c** is the absolute abundance distribution of key genera, and Fig d is the NMDS

that they could convert non-aromatic low-molecule substances into aromatic compounds, and a certain amount of aromatic compounds could be in turn further polymerized into humus macromolecular structure; another way was that part of refractory substances could be directly transformed into humus macromolecular structures, through the metabolic activity of key microbes. Therefore, the increased humus content in MBC treatments might be driven by the increase of key microbes.

#### 4 Conclusions

This study first revealed the effect of  $MnO_2$ -biochar composites on the humification during composting. Results showed that  $MnO_2$ -biochar composites could drive key microbial metabolic activity to accelerate humification processes. Therefore, they could be better utilized to enhance humification in composting. For this, this paper offers a more comprehensive theoretical foundation. This study exclusively investigated the influence of MBC on humification during chicken manure composting.

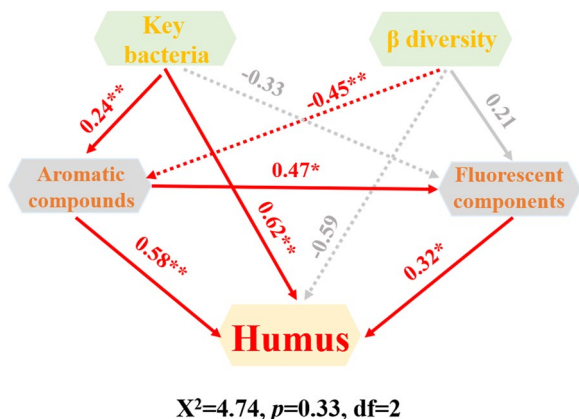


**Fig. 5** Causal relationships among key bacteria and the humification index are illustrated using a structural equation model. The thickness of the streamlines indicates the strength of the influences

In addition, MBC also exhibited exceptionally strong adsorption capability. Therefore, future research will comprehensively assess the impact of MBC on chicken manure composting, including but not limited to greenhouse gas reduction and hazardous waste treatment.

## Supplementary Information

The online version contains supplementary material available at <https://doi.org/10.1007/s42773-024-00315-4>.

**Additional file 1. Fig. S1** Scanning electron microscopy. a biochar and b MnO<sub>2</sub>-biochar. **Fig. S2.** Changes in temperature of the composting reactor. **Fig. S3.** Change in F<sub>max</sub> value of humic acid during composting of chicken manure and rice straw. In the Fig, a, b, c, d, and e represent CK groups, B, M, M+B, and MBC groups, respectively. **Fig. S4.** FTIR spectra of humic acid during composting. **a** CK and **b** MBC treatments. **Table S1.** The physicochemical characteristic of raw materials.

## Acknowledgements

Funding from the National Natural Science Foundation of China is gratefully acknowledged.

## Author contributions

All authors contributed to the study conception and design. Material preparation, data collection and analysis were performed by HQ, WG, LX, GZ, CS, ZW, NH, and TL. The first draft of the manuscript was written by HQ and all authors commented on previous versions of the manuscript. All authors read and approved the final manuscript.

## Funding

This work is funded by the National Key Research and Development Project (NO.2019YFC1906403), the National Natural Science Foundation of China [Grant numbers: 51978131, 523701486, 52370148, 52300161], and the Guangxi Natural Science Fund [Grant number: AD23026037].

## Data availability

The datasets used or analyzed during the current study are available from the corresponding author on reasonable request.

## Declarations

## Competing interests

The authors have no relevant financial or non-financial interests to disclose. The authors have no competing interests to declare that are relevant to the content of this article. All authors certify that they have no affiliations with or involvement in any organization or entity with any financial interest or non-financial interest in the subject matter or materials discussed in this manuscript. The authors have no financial or proprietary interests in any material discussed in this article.

## Author details

<sup>1</sup>Tianjin Key Laboratory of Animal and Plant Resistance, College of Life Sciences, Tianjin Normal University, Tianjin 300387, China. <sup>2</sup>School of Life Sciences, Liaoning University, Shenyang 110362, China. <sup>3</sup>College of Life Science, Liaocheng University, Liaocheng 252000, China. <sup>4</sup>School of Food and Biological Engineering, Hezhou University, Hezhou 542899, China.

Received: 31 August 2023 Revised: 27 February 2024 Accepted: 2 March 2024

Published online: 28 March 2024

## References

- Awasthi MK, Wang Q, Chen HY, Wang MJ, Ren XN, Zhao JC, Li J, Guo D, Li DS, Awasthi SK, Sun XN, Zhang ZQ (2017) Evaluation of biochar amended biosolids co-composting to improve the nutrient transformation and its correlation as a function for the production of nutrient-rich compost. *Bioresour Technol* 237:156–166
- Chen H, Awasthi SK, Liu T, Duan Y, Ren X, Zhang Z, Pandey A, Awasthi MK (2020) Effects of microbial culture and chicken manure biochar on compost maturity and greenhouse gas emissions during chicken manure composting. *J Hazard Mater* 389:121908
- Chen XM, Du Z, Liu D, Wang LQ, Pan CN, Wei ZM, Jia LM, Zhao R (2022) Biochar mitigates the biotoxicity of heavy metals in livestock manure during composting. *Biochar* 4(1):48
- El-Naggar AL, Mosa A, Ahmed N, Niazi NK, Yousaf B, Sarkar B, Rinklebe J, Cai YJ, Chang SX (2022) Modified and pristine biochar for remediation of chromium contamination in soil and aquatic systems. *Chemosphere* 303:134942
- Gao XT, Tan WB, Zhao Y, Wu JQ, Sun QH, Qi HS, Xie X, Wei ZM (2019) Diversity in the mechanisms of humin formation during composting with different materials. *Environ Sci & Technol* 53:3653–3662
- Hardie AG, Dynes JJ, Kozak LM, Huang PM (2009) The role of glucose in abiotic humification pathways as catalyzed by birnessite. *J Mol Catal A-Chem* 308:114–126
- He XS, Xi BD, Li X, Pan HW, An D, Bai SG, Li D, Cui DY (2013) Fluorescence excitation-emission matrix spectra coupled with parallel factor and regional integration analysis to characterize organic matter humification. *Chemosphere* 93:2208–2215
- He X, Hu Q, Chen JL, Leong WQ, Dai YJ, Wang CH (2022) Energy and environmental risk assessments of poultry manure sustainable solution: an industrial case study in Singapore. *J Clean Prod* 339:130787
- Ji ZY, Zhang LY, Liu YW, Li XQ, Li ZJ (2023) Evaluation of composting parameters, technologies and maturity indexes for aerobic manure composting: a meta-analysis. *Sci Total Environ* 886:163929
- Kasera N, Hall S, Kolar P (2021) Effect of surface modification by nitrogen-containing chemicals on morphology and surface characteristics of N-doped pine bark biochars. *J Environ Chem Eng* 9:105161
- Liang J, Liu J, Yuan X, Dong H, Zeng G, Wu H, Wang H, Liu J, Hu S, Zhang S, Yu Z, He X, He Y (2015) Facile synthesis of alumina-decorated multi-walled carbon nanotubes for simultaneous adsorption of cadmium ion and trichloroethylene. *Chem Eng J* 273:101–110
- Liang C, Schimel JP, Jastrow JD (2017a) The importance of anabolism in microbial control over soil carbon storage. *Nat Microbiol* 2:17105
- Liang J, Li X, Yu Z, Zeng G, Luo Y, Jiang L, Yang Z, Qian Y, Wu H (2017b) Amorphous MnO<sub>2</sub> modified biochar derived from aerobically composted swine manure for adsorption of Pb(II) and Cd(II). *ACS Sustain Chem Eng* 5:5049–5058
- Liu J, Yang X, Liu H, Cheng W, Bao Y (2020a) Modification of calcium-rich biochar by loading Si/Mn binary oxide after NaOH activation and its adsorption mechanisms for removal of Cu(II) from aqueous solution. *Colloid Surfaces A* 601:124960
- Liu YX, Gao CX, Wang YY, He LL, Lu HH, Yang SM (2020b) Vermiculite modification increases carbon retention and stability of rice straw biochar at different carbonization temperatures. *J Clean Prod* 254:120111
- Lodygin ED, Beznosikov VA, Vasilevich RS (2014) Molecular composition of humic substances in tundra soils (C-13-NMR spectroscopic study). *Eurasian Soil Sci* 47:400–406
- Lyu HH, Zhang QR, Shen BX (2020) Application of biochar and its composites in catalysis. *Chemosphere* 240:124842
- Oldfield TL, Sikirica N, Mondini C, Lopez G, Kuikman PJ, Holden NM (2018) Biochar, compost and biochar-compost blend as options to recover nutrients and sequester carbon. *J Environ Manage* 218:465–476
- Pan CN, Yang HY, Gao WF, Wei ZM, Song CH, Mi JY (2024) Optimization of organic solid waste composting process through iron-related additives: A systematic review. *J Environ Manage* 351:119952
- Qi H, Zhang A, Du Z, Wu J, Chen X, Zhang X, Zhao Y, Wei Z, Xie X, Li Y, Ye M (2021) delta-MnO<sub>2</sub> changed the structure of humic-like acid during co-composting of chicken manure and rice straw. *Waste Manage* 128:16–24
- Rajakpasha AU, Chen SS, Tsang DCW, Zhang M, Vithanage M, Mandal S, Gao B, Bolan NS, Ok YS (2016) Engineered/designer biochar for contaminant removal/immobilization from soil and water: potential and implication of biochar modification. *Chemosphere* 148:276–291

- Shaheen SM, Natasha, Mosa A, El-Naggar A, Hossain MF, Abdelrahman H, Niazi NK, Shahid M, Zhang T, Tsang YF, Trakal L, Wang S, Rinklebe J (2022) Manganese oxide-modified biochar: production, characterization and applications for the removal of pollutants from aqueous environments a review. *Bioresour Technol* 346:126581
- Song BA, Yin Z, Almatrafi E, Sang F, Shen MC, Xiong WP, Zhou CY, Liu Y, Zeng GM, Gong JL (2022) When chicken manure compost meets iron nanoparticles: an implication for the remediation of chlorophenothane-polluted riverine sediment. *Environ Sci-Nano* 9:1519–1529
- Sun R, Zhu XD, Wang C, Yue JY, Pan LN, Song CH, Zhao Y (2024) Effect of NH<sub>4</sub><sup>+</sup> and NO<sub>3</sub><sup>-</sup> cooperatively regulated carbon to nitrogen ratio on organic nitrogen fractions during rice straw composting. *Bioresour Technol* 395:13031
- Wang YD, Hu N, Ge TD, Kuzyakov Y, Wang ZL, Li ZF, Tang Z, Chen Y, Wu CY, Lou YL (2017) Soil aggregation regulates distributions of carbon, microbial community and enzyme activities after 23-year manure amendment. *Appl Soil Ecol* 111:65–72
- Wu D, Yue JY, Gao WF, Wang F, Qu FT, Song CH, Wei ZM (2024) Functional genes are the key factors driving the Fenton-like reactions to promote the hydrolysis of lignocellulosic biomass during composting. *Ind Crop Prod* 210:118131
- Xiong SG, Liu YD, Zhang H, Xu SQ, Li SR, Fan XQ, Chen R, Ding GC, Li J, Wei YQ (2023) Effects of chemical additives and mature compost on reducing nitrogen loss during food waste composting. *Environ Sci Pollut R* 30:39000–39011
- Yang WQ, Zhuo Q, Chen QH, Chen ZL (2019) Effect of iron nanoparticles on passivation of cadmium in the pig manure aerobic composting process. *Sci Total Environ* 690:900–910
- Yuan Y, He XS, Xi BD, Li D, Gao RT, Tan WB, Zhang H, Yang C, Zhao XY (2018) Polarity and molecular weight of compost-derived humic acid affect Fe(III) oxides reduction. *Chemosphere* 208:77–83
- Zhang M, Gao B, Yao Y, Xue Y, Inyang M (2012) Synthesis of porous MgO-biochar nanocomposites for removal of phosphate and nitrate from aqueous solutions. *Chem Eng J* 210:26–32
- Zhang CY, Li X, Zhao XY, Yang JJ, Li SK, Dang QL, Tan XK (2022a) Recognize and assessment of key host humic-reducing microorganisms of antibiotic resistance genes in different biowastes composts. *Sci Total Environ* 806:150736
- Zhang YY, He MJ, Wang L, Yan JH, Ma B, Zhu XH, Ok YS, Mechtcherine V, Tsang DCW (2022b) Biochar as construction materials for achieving carbon neutrality. *Biochar* 4:59
- Zhang Y, Xu Y, Li J, Chen G, Wang S, Xu Y, Xu R, Zhang B, Zhang H (2023) Microbial metabolism and humic acid formation in response to enhanced copper and zinc passivation during composting of wine grape pomace and pig manure. *Bioresour Technol* 384:129226
- Zhao M, Cai C, Yu Z, Rong H, Zhang C, Zhou S (2022a) Effect of biochar on transformation of dissolved organic matter and DTPA-extractable Cu and Cd during sediment composting. *Environ Sci Pollut R* 29:27977–27987
- Zhao XY, Xu KL, Wang JW, Wang ZQ, Pan RK, Wang Q, Li SL, Kumar S, Zhang ZQ, Li RH (2022b) Potential of biochar integrated manganese sulfate for promoting pig manure compost humification and its biological mechanism. *Bioresour Technol* 357:127350